Wave-Absorbing Controllers for a Flexible Beam

A.H. von Flotow* and B. Schäfer†
Deutsche Forschungs- und Versuchsanstalt für Luft- und Raumfahrt, Federal Republic of Germany

This paper describes theoretical and experimental work performed on the modelling and vibration control of a hanging flexible beam. The synthesis and laboratory implementation of low-authority controllers based upon feedback of local velocity to actuator force has been the subject of previous studies. This paper extends this work with the design and laboratory implementation of low-authority controllers based upon concepts of disturbance propagation and reflection. Control forces are applied to the lower end of the hanging beam. Compensators are derived which feed back local deflection and slope to control force and moment with the goal of minimizing the reflection of energy at the lower end. Several of these compensators are approximated by analog electronic filters for laboratory implementaion. The performance of these wave-absorbing compensators is compared with that of velocity feedback.

I. Introduction

OVER the past five years, a trend has developed to divide the problem of control of flexible structures conceptually in two. It has been recognized[1] that several characteristics of the dynamics of flexible structures (uncertainty in the model, and the very large number of lightly damped modes participating in the response) make a direct approach to full-state estimation and feedback impractical. It is too easy to destabilize lightly damped and poorly modelled structural modes. The modes in greatest danger of being destabilized are typically those at, or just beyond, the bandwidth of such a "full state" controller.

One approach to alleviate these difficulties is damping augmentation of the structure, by both passive and active means. Active damping augmentation has been termed[2] "low-authority" control, and has been achieved by direct velocity feedback of colocated sensors and actuators[3] and dislocated sensors and actuators.[4] Actuator and sensor dynamics can lead to destabilization of modes near the bandwidth of the actuator or sensor.[5] A certain minimum amount of passive damping must be present to avoid such destabilization.

An alternative approach to low-authority control has been developed recently.[6,7] This alternative begins with the viewpoint that, in many cases, it may be profitable to view the response of a flexible structure to a typical locally applied force in terms of travelling elastic distubances. This view is especially apt with respect to large spacecraft structures, where the predominant forces acting upon the structure are spatially and temporally localized. Typically the largest forces will originate on board, and would be due to thruster firing, rotating imbalanced machinery, and other sources.[8]

This point of view leads naturally to the thought that it may be possible to actively modify the natural disturbance paths within the structure, and to shunt or otherwise direct this energy at will. Computational examples[6] suggest that such controllers, if realizable, can deliver amazing performance. In particular, it may be possible to design active controllers that act as perfect "wave absorbers," "swallowing" all energy incident upon them, and in simple structures (beams and rods), moving every structural pole to infinity.

This paper describes the theoretical development and experimental implementation of such wave absorbers for a particular experimental structure, the hanging clamped-free flexible beam. This structure, and the performance of low-authority controllers based upon direct velocity feedback with colocated and noncolocated sensors and actuators, has been described previously.[9] The wave absorber is applied to the lower (free) end of the beam and feeds back local deflections to local forces. The compensators used are derived from the point of view of minimizing reflected energy, and are in general infinite dimensional and infinite in bandwidth. Because of practical laboratory limitations (approximation of the infinite dimensional compensator, finite bandwidth actuator and sensor, and the availability of only force actuators rather than torquers), this absorption of energy cannot be perfect.

A surprising result of both the theoretical and the experimental work is the similarity between the new wave-absorbing compensators and the previous velocity feedback. The wave-absorbing compensators specified by the theory can be viewed as velocity feedback modified to have slightly a different phase, and gain increasing with frequency.

II. Analysis of the Flexible Beam and Compensator Synthesis

Beam Dynamical Model

The beam (Fig. 1) consists of a stainless steel sheet of thickness 1 mm, width 10 cm, and length 2.9 m. It is supported by a massive I-beam weighing approximately 500 kg. The support structure has lowest natural frequencies of about 56 and 82 Hz.

The predominant flexibility of the beam leads to horizontal deflections, $w(x,t)$, in only one plane. This behavior is well described by the partial differential equation (damping is ignored)

$$\tilde{EI}\frac{\partial^4 w}{\partial x^4}-\frac{\partial}{\partial x}\left(S\frac{\partial w}{\partial x}\right)+\rho A\frac{\partial^2 w}{\partial t^2}=F(x,t) \tag{1}$$

together with the boundary conditions

$$w(0,t)=0 \qquad \tilde{EI}\frac{\partial^2 w}{\partial x^2}(l,t)=M_c$$

$$\frac{\partial w}{\partial x}(0,t)=0 \qquad \tilde{EI}\frac{\partial^3 w}{\partial x^3}(l,t)=V_c \tag{2}$$

Presented as Paper 85-1922 at the AIAA Guidance, Navigation and Control Conference, Snowmass, CO, Aug. 19-21, 1985; received Sept. 18, 1985; revision received Feb. 6, 1986.

*Guest Scientist. Member AIAA.
†Staff Research Scientist.

where $S(x)=\rho Ag(l-x)$ is the tensile force due to gravity acting upon the uniform beam, $\tilde{E}$ the effectie Young's modulus, I the cross-sectional moment of inertia, ρ the mass density of the beam material, and A the cross-sectional area of the beam. The external force $F(x,t)$ does not include the control torque M_c and control force V_c applied to the tip of the beam. These are included in the boundary conditions.

A modal analysis and experimental identification of the structure had been performed. This analysis[9] applied Galerkin's method[10] to the partial differential Eq. (1), using as trial functions the gravity-free cantilever beam eigenfunctions. Open-loop eigenfrequencies and mode shapes were calculated in this manner, using 20 trial functions. An important result of this modelling effort was the determination that actual material stiffness seemed to be approximately 20% lower than the expected value of 2×10^{11} N/m^2. Therefore the modified Young's modulus, $\tilde{E}$, given in Fig. 1 was determined such that the five lowest natural frequencies agree very well with the corresponding experimental data. Since density can be measured easily, it is assumed that the entire discrepancy is due to Young's modulus.

Modal-Based Controller Design

The design and implementation of modal-based low-authority controllers for this beam is the subject of a previous paper.[9] In these designs, lateral velocity of the beam at selected points is fed back to force actuators. The magnitude of the feedback gains and the position of the sensors and actuators are design variables which were optimized. Various sensor and actuator locations were studied analytically and experimentally.

For the purpose of comparison with the wave absorbing controllers in this study, only the modal controller using colocated sensing and actuating at the tip of the beam will be considered. This modal controller has the most similarity with the wave-absorbing contollers, and performs as well as any of the modal-based controllers tested. The feedback gain of this controller was chosen by an optimization routine,[9] maximizing the fraction of the energy dissipated by contol action, during vibration decay from some initial condition. This gain is 3.96 N-s/m.

It is interesting that the value of this "optimium" feedback gain depends upon the initial conditions. If high-frequency modes are strongly excited, the optimizer raises the velocity feedback gain. If low-frequency modes are strongly excited, the optimizer reduces the velocity feedback gain.[4,9] The value of 3.96 N-s/m is a compromise, obtained using the lowest five modes in the modal controller design, with initial conditions produced by an impact at $x/l=0.2$

Wave-Absorbing Controller Design

To describe the design of a wave-absorbing controller, it is first necessary to discuss the beam dynamics in terms of travelling waves. Such an analysis is much simplified by the assumption that the tension, S, can be ignored. Since the tension is variable with x, wave amplitudes, speeds, and wavelengths are functions of axial position x. The analysis is then best carried out via the WKB perturbation method,[11] or numerically. A further argument supporting the decision to ignore the tension is that its influence becomes less and less important at high frequencies, exactly in the region where a low-authority controller must be effective. Also, the tension is zero at the tip, and it is only the local dynamics at the tip which influence the performance of a wave-absorbing contoller.

With this simplification, the analysis proceeds with the introduction of the cross-sectional state vector $y=(w,\theta,M,V)^T$, where $\theta=\partial w/\partial x$ is the slope, $M=\tilde{E}I(\partial^2 w/\partial x^2)$ is the internal bending moment and $V=\tilde{E}I(\partial^3 w/\partial x^3)$ is the internal shear force. The sign conventions are given in Fig. 1. If the partial differential Eq. (1) is Fourier-transformed (in order to avoid new symbols, the transformed variables hereafter have the same notation as their time-dependent equivalents), the beam dynamics are described by the equation

$$\frac{dy}{dx}=\begin{bmatrix}0&1&0&0\\0&0&\frac{1}{\tilde{E}I}&0\\0&0&0&1\\\omega^2\rho A&0&0&0\end{bmatrix}y+\begin{bmatrix}0\\0\\0\\F(x,\omega)\end{bmatrix} \tag{3}$$

To describe the separate processes of wave propagation and wave generation by external forces, it is convenient to set $F(x,w)=0$ in Eq. (3), and to include external point forces in boundary conditions.

Equation (3) is diagonalized by the transformation

$$y=\begin{bmatrix}1&1&1&1\\-i\Theta_0&-\Theta_0&i\Theta_0&\Theta_0\\-M_0&M_0&-M_0&M_0\\iV_0&-V_0&-iV_0&V_0\end{bmatrix}w=Y(\omega)w \tag{4}$$

where $i=\sqrt{-1}$, $\Theta_0=\sqrt{\omega/a}$, $M_0=\omega\sqrt{\rho A\tilde{E}I}$, $V_0=\Theta_0 M_0$ and $a=\sqrt{\tilde{E}I/\rho A}$.

This diagonalization may be interpreted in terms of travelling waves. Each entry of the new cross-sectional state vector w is the amplitude of a travelling wave mode. These wave modes consist of frequency-dependent combinations of physical cross-sectional state variables, the columns of matrix Y, and travel independently of one another along the beam. The amplitudes of these wave modes vary according to

$$\frac{dw}{dx}=\begin{bmatrix}-i\sqrt{\omega/a}&&&\\&-\sqrt{\omega/a}&&\\&&i\sqrt{\omega/a}&\\&&&\sqrt{\omega/a}\end{bmatrix}w \tag{5}$$

The entries of the matrix in Eq. (5) are propagation coefficients, $\gamma(\omega)=\alpha(\omega)+ik(\omega)$, of the uniform Bernoulli-Euler beam. The real part, $\alpha(\omega)$, is the attenuation coefficient, the imaginary part, $k(\omega)$, is the wave number. These propagation coefficients come in pairs, $(\gamma_j,-\gamma_j)$, corresponding to similar wave modes travelling in opposite directions. The principle of conservation of energy restricts these propagation coefficients to the first and third quadrants of the complex γ-plane.

The cross-sectional state vector w has been ordered (notation from the literature of microwave circuits[12]), $w=(a_1, a_2,b_1,b_2)^T$, where a_1 and a_2 are the amplitudes of wave modes travelling toward the lower end of the beam, and b_1 and b_2 are wave modes departing the lower end of the beam. Inspection of Eq. (5) reveals a_2 and b_2 to be "near fields." Their

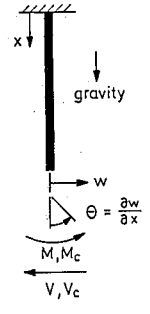

Beam Characteristics

material	austenitic stainless steel
length	2.9 m
width	0.1 m
thickness	1.0 mm
density	8.0 g/cm^3
modulus	$1.60\cdot10^{11}$ N/m^2
Poisson's ratio	0.3

Fig. 1 Flexible beam model with sign conventions and beam characteristics.

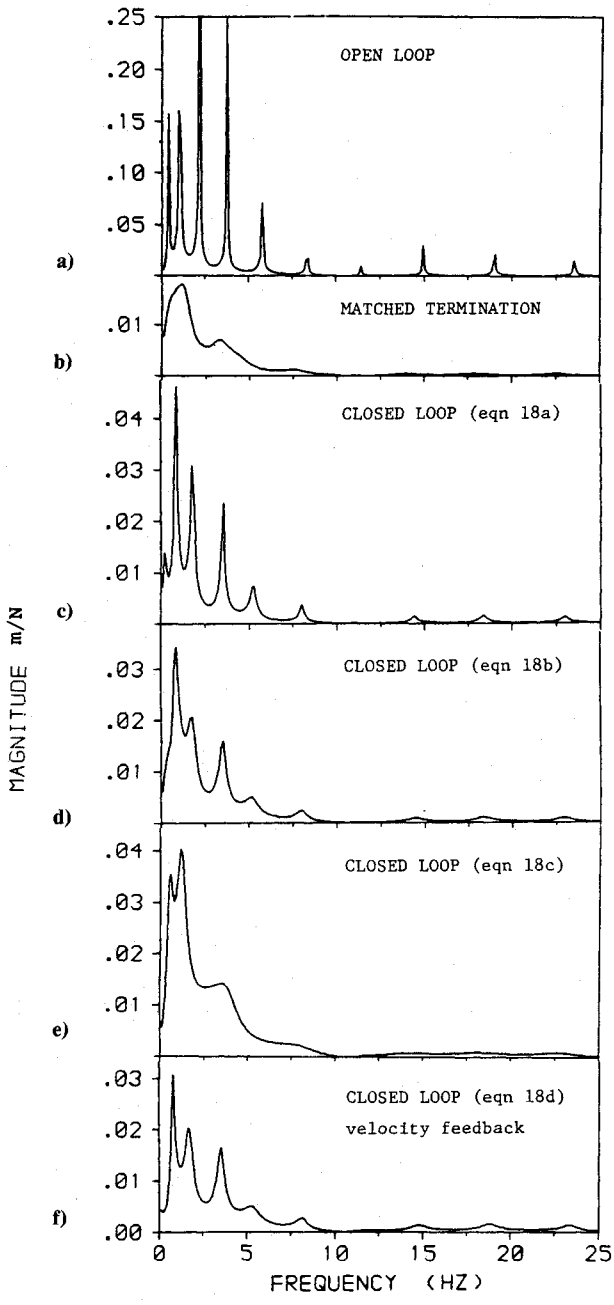

Fig. 2 Calculated open (a) and closed loop (b-f) structural responses (force excitation at $x/l=0.2$, deflection measurement at tip, $x/l=1.0$) for different compensator designs.

amplitude decays exponentially with x. The characteristic length of these near fields is $\sqrt{a/\omega}$, or for this particular beam ($a=1.35$ m^2/s), less than 0.5 m for frequencies greater than 1 Hz. Since the beam is 2.9 m long, one might expect these near fields to contribute very little to the dynamics above 1 Hz.

To complete the description of the beam dynamics in wave-mode coordinates, the boundary conditions in terms of the state vector y and the externally applied (control) force V_c and torque M_c are introduced

$$\begin{bmatrix} 0 & 0 & 1 & 0 \\ 0 & 0 & 0 & 1 \end{bmatrix} y(l,\omega) = \begin{pmatrix} M_c \\ V_c \end{pmatrix} \tag{6}$$

and transformed into wave-mode coordinates;

$$\begin{bmatrix} -M_0 & M_0 & -M_0 & M_0 \\ iV_0 & -V_0 & -iV_0 & V_0 \end{bmatrix} w(l,\omega) = \begin{pmatrix} M_c \\ V_c \end{pmatrix} \tag{7}$$

Partitioning into incoming a_j, and outgoing, b_j, wave modes and inversion of a 2×2 matrix leads to the result

$$\begin{pmatrix} b_1 \\ b_2 \end{pmatrix} = \begin{bmatrix} \frac{i+1}{i-1} & \frac{-2}{i-1} \\ \frac{2i}{i-1} & -\frac{i+1}{i-1} \end{bmatrix} \begin{pmatrix} a_1 \\ a_2 \end{pmatrix} + \begin{bmatrix} \frac{1}{M_0(i-1)} & \frac{-1}{V_0(i-1)} \\ \frac{i}{M_0(i-1)} & \frac{-1}{V_0(i-1)} \end{bmatrix} \begin{pmatrix} M_c \\ V_c \end{pmatrix} \tag{8}$$

or, in general,

$$\boldsymbol{b} = \boldsymbol{S}\boldsymbol{a} + \boldsymbol{B}\boldsymbol{F}_{\mathrm{EXT}} \tag{9}$$

Equation (8) is the boundary condition (6), expressed in casual form. Outgoing wave modes, $\boldsymbol{b}$, are produced by reflection of the incoming wave modes, $\boldsymbol{a}$, and are generated by control forces and moments. The scattering matrix, $\boldsymbol{S}$, is a matrix of reflection coefficients.

Equation (8) is the basis for designing wave absorbing controllers to be applied to the beam tip. In this work such controllers were limited to the form

$$\begin{pmatrix} M_c \\ V_c \end{pmatrix} = \boldsymbol{C}(\omega) \begin{pmatrix} w \\ \theta \end{pmatrix}_{\mathrm{TIP}} \tag{10}$$

applying tip force and torque in response to tip deflection and slope. The compensator matrix, $\boldsymbol{C}$, is generally full.

For evaluation and design of various compensators of the form of Eq. (10), it is convenient to derive an expression for the closed loop scattering matrix, $\boldsymbol{S}_{\mathrm{CL}}$, giving $\boldsymbol{b}=\boldsymbol{S}_{\mathrm{CL}}\boldsymbol{a}$. This expression comes from Eq. (10), (9) and (4)

$$S_{CL} = \left\{ I - BC \begin{bmatrix} 1 & 1 \\ i\Theta_0 & \Theta_0 \end{bmatrix} \right\}^{-1} \left\{ S + BC \begin{bmatrix} 1 & 1 \\ -i\Theta_0 & -\Theta_0 \end{bmatrix} \right\} \tag{11}$$

The Matched Termination

The compensator which leads to $S_{\mathrm{CL}}=0$ is termed a matched termination in the microwave literature. This compensator is just the driving point impedance of a semi-infinite beam:

$$\begin{pmatrix} M_c \\ V_c \end{pmatrix}_{\mathrm{MTCH}} = \begin{bmatrix} -iM_0 & -(1+i)M_0/\Theta_0 \\ (-1+i)V_0 & iM_0 \end{bmatrix} \begin{pmatrix} w \\ \theta \end{pmatrix}_{\mathrm{TIP}} \tag{12}$$

Substitution of this compensator into Eq. (11) confirms that the closed loop scattering matrix is zero.

The matched termination of Eq. (12) makes use of control torques, and requires measurement of tip slopes, but neither of these were readily available in the lab. Rather than insist upon the construction of a torque actuator and a slope sensor, the approach taken here was to derive compensators using only force actuation and deflection measurements. Several approaches are possible. One is to use only the (2,1) element of the matched termination, applying control forces only in response to tip deflection. Alternatively, it is possible to derive wave-absorbing compensators while explicitly taking into account the laboratory limitations.

Other Wave-Absorbing Compensators (Using Only Force Actuation)

The Bernoulli-Euler beam model supports two wave modes, a travelling mode and a near field. As response frequencies increase, the near field contributes only marginally to the response. This leads to the thought that it may be clever to modify only the generation of the travelling mode, b_1, at the

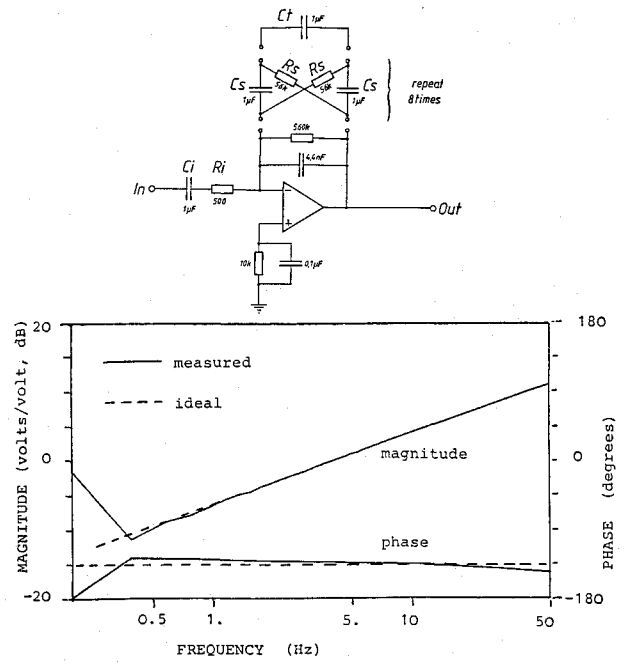

Fig. 3 A schematic diagram of the "half differentiating" circuit and its measured performance with eight cells in the feedback lattice.

beam tip. This idea leads to several different compensators, depending upon the assumptions made in their derivation.

Setting $b_1 = 0$ (no reflected travelling wave) and $M_c = 0$ (using only force actuation) in Eq. (8) leads to the compensator

$$V_c = [iV_0 \quad M_0]\,(w \quad \theta)^T_{\mathrm{TIP}}$$

A possible simplification is the use of only the tip deflection feedback term, $V_c = iV_0 w_{\mathrm{TIP}}$.

If one restricts the compensator matrix C to be non-zero only in the (2,1) element (only feedback tip deflection to control force), then Eq. (11) can be further expanded to yield

$$S_{\mathrm{CL}} = \begin{bmatrix} \dfrac{C_{21}(-i+1)-V_0}{C_{21}(i-1)-iV_0} & \dfrac{V_0(-i+1)}{C_{21}(i-1)-iV_0} \\ \dfrac{-V_0(i+1)}{C_{21}(i-1)-iV_0} & \dfrac{C_{21}(-i+1)+V_0}{C_{21}(i-1)-iV_0} \end{bmatrix} \tag{13}$$

Use of this expression allows one to influence individual terms of the closed-loops scattering matrix directly.

The compensation $V_c = \frac{1}{2}(1+i)V_0 w_{\mathrm{TIP}}$ leads to $S_{\mathrm{CL}}(1,1) = 0$. This is expected to be the reflection coefficient of predominant importance, since it describes the generation of outgoing travelling wave modes, b_1, by incident travelling wave modes, a_1.

An alternative is to set the determinant of the closed-loop scattering matrix S_{CL} to zero. The compensator that accomplishes this, using only the (2,1) term of the compensator matrix, is $V_c = -\frac{1}{2}(1-i)V_0 w_{\mathrm{TIP}}$.

Many other approximate wave-absorbing compensators are derivable. The equations listed above may be used as the starting point for their derivation.

Comparison of Synthesized Compensators

The previous discussion has made it clear that, apart from the unique matched termination, there are many wave-absorbing compensators that may be applied to the beam tip. Note that the phase of the compensators discussed in the previous section, feeding back only tip deflection to control force, is constant with frequency and within 45 deg of velocity feedback. The gain rises with frequency; its dependence is always $\sim\omega^{3/2}$. The gain of the optimal direct velocity feedback design is the same as that of these wave-absorbing compensators in the vicinity of 3 Hz. The phase of two of the wave-absorbing compensators implies positive damping but negative stiffness. Simulations of closed-loop structural response were used to further differentiate between these designs.

III. Structural Response Simulations

A truncated modal model of the structure was used to simulate the structural response rather than a wave-propagation model. This choice was made because of the availability of a well-validated model (modal identification of the beam had been very successful[9]), and to simplify the calculations. The first 10 structural modes were used in the simulation. In modal coordinates, the beam dynamics are described by

$$\rho Al[\Omega + i\omega D_0 - \omega^2 I]\,q = Q \tag{14}$$

where q is the vector of modal amplitudes, $\Omega = \mathrm{diag}(\omega_k^2)$ is the diagonal matrix of open-loop structural frequencies, $D_0 = \mathrm{diag}(2\xi_k\omega_k)$ gives the open loop modal damping ratios and Q is the vector of generalized modal forces. Modal damping ratios had been experimentally determined, and were 0.3% for the first, decreasing to less than 0.1% for the seventh and higher modes.

If the beam is excited by a lateral force $F(x_i,\omega)$ at x_i, the lateral deflection response w at x_0 is given by

$$\frac{w(x_0,\omega)}{F(x_i,\omega)} = [\Phi_1(x)\ldots\Phi_{10}(x)]_{x=x_0} D^{-1}(\omega) \begin{bmatrix} \Phi_1(x) \\ \vdots \\ \Phi_{10}(x) \end{bmatrix}_{x=x_i} \tag{15}$$

where $\Phi_i(x)$ is the ith mode shape, and the system dynamics matrix, $D(\omega)$, is the sum of the open-loop dynamics matrix and a modal coupling matrix due to the controller at the tip

$$D(\omega) = \rho Al[\Omega + i\omega D_0 - \omega^2 I] - \begin{bmatrix} \dfrac{d\Phi_1}{dx} & -\Phi_1 \\ \vdots & \vdots \\ \dfrac{d\Phi_{10}}{dx} & -\Phi_{10} \end{bmatrix} C(\omega) \begin{bmatrix} \Phi_1 & \Phi_{10} \\ \dfrac{d\Phi_1}{dx} & \dfrac{d\Phi_{10}}{dx} \end{bmatrix} \tag{16}$$

Due to the unusual frequency dependence of the compensator matrix $C(\omega)$, an eigenvalue solution for the closed-loop poles of Eq. (15) is not practical. The approach taken was to calculate the transfer functions (15) explicitly at many frequencies. This is computationally intensive, but makes minimum demands upon the programmer. If velocity feedback were used, a linear eigenvalue solution in the extended state variables $(q, dq/dt)^T$ would be possible.

Simulations with Ideal Compensators

Figures 2a-f present simulated responses for some of the compensators considered. Excitation is provided by a lateral force at $x/l = 0.2$; the response is calculated at $x/l = 1.0$. These positions were chosen to be the same as those used in a previous study.[9]

Inspection of these figures is instructive. Since the pole locations in the left-half s-plane were not determined, decisions about the quality of the closed-loop response must be made based upon these transfer functions. The degree of modal damping must be estimated (curve fitting could be used) from these transfer functions. The matched termination (Fig. 2b)

performs well. If one takes only the (2,1) term of the matched termination (Fig. 2c), the damping performance deteriorates strongly to a level inferior to that provided by the original direct velocity feedback (Fig. 2f). Setting the outgoing travelling wave mode to zero, $b_1 = 0$, yields well-damped structural responses. If one takes only the (2,1) term of this compensator, the closed-loop structural responses deteriorate to those of Fig. 2d, still "better" than the reference responses with direct velocity feedback (Fig. 2f). The best damping is provided by the compensator, which sets the (1,1) term of the tip reflection matrix to zero, $S(1,1) = 0$. Figure 2e shows these closed-loop responses.

Comparison of these simulated responses, and the laboratory restriction to force actuation and deflection sensing, suggested the laboratory verification of three wave-absorbing compensators corresponding to Eqs. (17a-c) of Sec. IV. These three compensators differ from each other only by a constant gain factor, and by constant phase shifts of 45 and 90 deg.

IV. Electronic Realization of the Compensator Transfer Functions

The compensators to be implemented all have a frequency-dependent gain, $V_c \sim \omega^{3/2} w_{TIP}$, and constant phase. The deflection signal from the optimal sensor is differentiated by an analog differentiation circuit. The signal also passes through a "half differentiating" filter which yield the $\omega^{1/2}$ amplitude and through a filter which attempts to modify the phase as required without greatly modifying the amplitude. The signal finally passes through an amplifier which takes into account the sensor, actuator and other circuit gains to yield the required overall compensator gain. In practice, it proved to be necessary to introduce several low-pass filters and to provide first-order roll-off for both differentiators to help control noise. These measures contributed to the phase lag of the entire network.

This approach to compensator design, i.e. cascading several filters with independent design goals, is pehaps not the best approach to the circuit design problem. An alternative would be to derive Padé or other rational approximations to the entire required compensator. These rational approximations would then be approximately realized by analog circuits or algorithms on a digital computer. This approach was not taken in this study for several reasons. First, a filter design was known, and had been tested, which yielded the $\omega^{1/2}$ amplitude dependence; thus it was only necessary to design the required phase-shifting filters. Second, the approach taken has the benefit of breaking the filter design problem into separate subproblems, each with its own clear design goal. For wave-absorbing and wave-shunting compensators of greater complexity,[6] it may be necessary to adopt another design approach.

To clarify the following sections, it is convenient to explicitly give the various compensators to be implemented. The compensators are (with units of Newtons for V_c, meters for w_{TIP}, and radians per second for ω).

From the matched termination:

$$V_c = (1+i)\omega^{3/2} 0.929 w_{TIP} \tag{17a}$$

From $b_1 = 0$ with V_c only:

$$V_c = i\omega^{3/2} 0.929 w_{TIP} \tag{17b}$$

From $S_{CL}(1,1) = 0$ with V_c only:

$$V_c = \tfrac{1}{2}(1+i)\omega^{3/2} 0.929 w_{TIP} \tag{17c}$$

Optimized direct velocity feedback:

$$V_c = i\omega 3.96 w_{TIP} \tag{17d}$$

Direct velocity feedback [Eq. (17d)] is the easiest to implement. The output of the differentiator is lead, via an amplifier, directly to the actuator.

The "Half Differentiator"

A circuit which yields an $(i\omega)^{1/2}$ behaviour is given in Fig. 3, together with measured performance. It was proposed by Vaughan[13] for use in vibration control of beams, but was apparently first proposed by Carlson and Halijak.[14] Its unusual peformance is based upon the relatively well-known fact that the characteristic impedance of an R-C lattice such as the one in Fig. 3 is $1/\sqrt{i\omega R_s C_s}$. Thus use of this lattice as the feedback network of an operational amplifier can yield "half integrators" as well. To implement a "half differentiator," one uses a capacitor as the input impedance of the operational amplifier; to implement a "half integrator," one uses a resistor. A resistor has been included in the input of the operational amplifier to roll off the bahaviour at 500 Hz and turn the circuit into a "half integrator" at high frequencies. The frequency at which the circuit most closely yields the desired bahaviour (given by $C_s R_s$) was set at 3 Hz. Eight cells were used in the feedback lattice, an arbitrary choice. The gain is seen to follow the $\omega^{1/2}$ frequency behavior very closely, while the phase exhibits some variation.

Phase Shift Filters

Cascading a differentiator and the "half differentiator" of the previous section theoretically yields the compensator of Eq. (17a). In practice, the low-pass filters used to control noise introduce a phase lag, increasing with frequency. The compensators of Eqs. (17b) and (17c) differ from that of Eq. (17a) by constant phase shifts of 45 and 90 deg, respectively. Thus, phase-shifting networks are required to lag the phase by a constant amount without disturbing the amplitude. This should be achieved over the dominant structural response-frequency range from 0.1 to 20 Hz. Further, the phase-shifting network may not destroy the phase or gain too severely outside of this frequency range.

Such performance can only be provided approximately. Theoretical and practical limitations on such filters have been

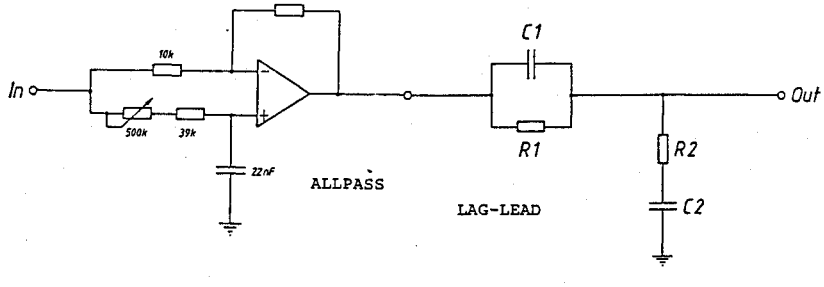

Fig. 4 The phase shifting circuit: a first-order allpass and a lag-lead network.

discussed by Hermann.[15,16] He has proposed rational allpass filter transfer functions to approximate the function $e^{i(\pi/2)sgn(\omega)+t_{LAG}\omega}$, where the lag t_{LAG} is introduced to make the filters realizable. These filters approximate this transfer function in a Chebyshev sense. Extrapolation of Herrmann's results suggests that to achieve the desired phase to within 10 deg over a fequency range of two decades would require an allpass of order 17.

The design and implementation effort of the approach of Herrmann goes well beyond the level envisaged for this work. The approach taken was to sacrifice some amplitude fidelity to achieve the required phase shift with much simpler filters. Figure 4 shows the circuitry used to implement the phase-shifting filter. It consists of a first-order allpass cascaded with a lag-lead network. The allpass has unit gain and a phase which decreases monotonically from 0 to -180 deg, while the lag-lead filter has a phase which improves upon that of the allpass, but an amplitude which departs from unity. To compensate for gain variations, the compensator amplifier is varied by an additional factor K_p.

This phase-shifting filter is thus defined by five parameters: the allpass characteristic frequency, three lag-lead characteristic frequencies, and the additional amplifier gain. The corresponding transfer function is

$$\frac{e_0}{e_i} = K_P \underbrace{\frac{1-i\omega T_a}{1+i\omega T_a}}_{\text{allpass}} \underbrace{\frac{(1+i\omega T_1)(1+i\omega T_2)}{(1+i\omega T_1)(1+i\omega T_2)+i\omega T_3}}_{\text{lag-lead}} \tag{18}$$

where e_0 denotes the output and e_i the input signal; K_p is the additional gain of the compensator amplifier, $T_a = R_a C_a$ is the time constant of the allpass, and $T_1 = R_1 C_1$, $T_2 = R_2 C_2$ and $T_3 = R_1 C_2$ are the three time constants of the lag-lead filter.

The compensator is completed by one final amplifier, whose gain is chosen to compensate for the scale factors of the sensor and of the actuator, and to negate the 1/10 attenuation performed by the differentiating filter.

V. Experimental Results

Experimental Hardware and Procedure

The experimental structure has been described in Sec. II. The actuators and sensors were only briefly mentioned, and are best described more thoroughly.

The optical displacement sensor is a commercially available device (ELAG Elektronik, Winterthur, Switzerland). Its operation is based upon the triangulation principle. A laser diode illuminates the target; the distance to the illuminated spot is measured with a resolution of 0.05% over a range of ± 16 mm. A dedicated microprocessor linearizes the output to within 0.4%. The bandwidth is 2kHz.

The force actuator was developed in-house at the DFVLR. It employs a pair of coils to apply electrodynamic forces to a pair of permanent magnets with a combined mass of 50 gm. The resolution is better than 1% over the range ± 1.1 N, and non-linearity is below 1% over a displacement range of ± 12 mm. The bandwidth is extended to 200 Hz by a current-sensing feedback loop. This amplifier design ensures that the electromagnetic force applied to the magnet pair is as commanded, and is independent of velocity-induced back voltage. However, the force applied to the beam is modified by the mass loading of the magnets. The magnitude of this effect was not realized until pointed out in review.

The inertial force of the magnets on the beam varies with ω^2 and leads the control force (which varies with $\omega^{3/2}$) by 45 to 135 deg. The magnitudes become equal at approximately 70 Hz. Although it may, in principle, be possible to actively compensate for this mass loading, this was not attempted. Although this omision will be important at high frequencies, the effect is not overly important below 25 Hz.

All measurements were performed with a Hewlett-Packard 5423 A structural dynamics analyzer. This instrument can be used to calculate, manipulate, and display transfer functions of two input signals. The instrument also provides a noise source, suitable for use as an excitation signal in lightly damped systems. This noise source was used as the excitation signal in all the measurements performed.

Once the electronic filters had been tested, they were connected to the beam via the tip actuator and sensor. The spectrum analyzer was then connected to the disturbance force actuator at $x/l = 0.2$. Displacement measurements were made at the tip, $x/l = 1.0$.

Experimental Results

Figure 5 shows a measured open loop structural transfer function. This figure may be compared directly with Fig. 2a. Figures 6-9 show various compensator transfer functions in volts per volt. These compensators were connectd to the beam with combined sensor and actuator gains of 28.6 N/m.

Figure 6 summarizes velocity feedback, displaying both the compensator and a closed-loop transfer function. The closed

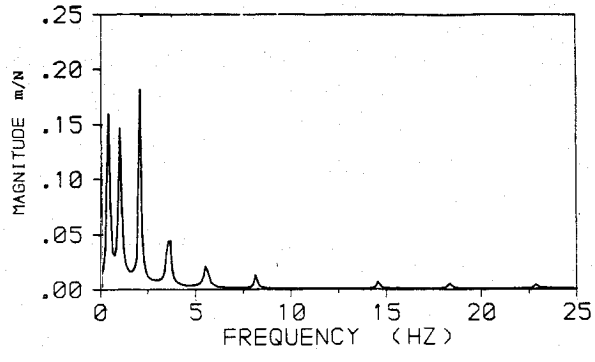

Fig. 5 Measured open-loop transfer function (force excitation at $x/l = 0.2$, measured deflection at $x/l = 1.0$). Compare with Fig. 2a.

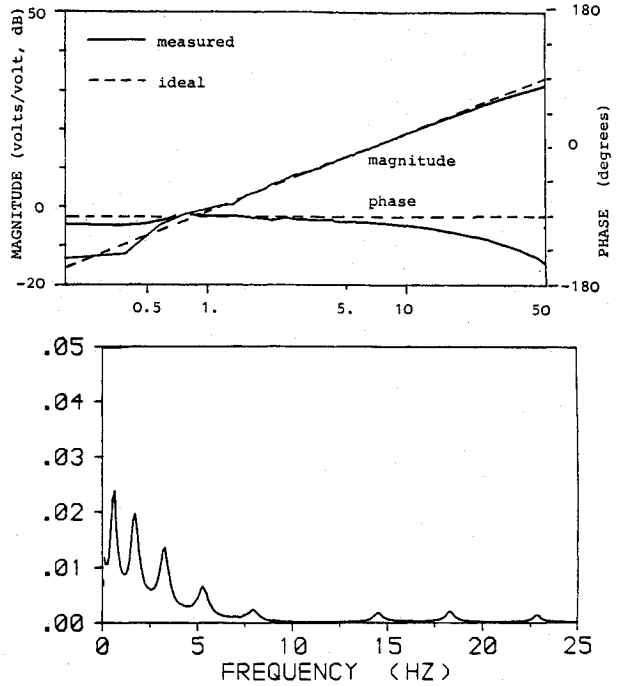

Fig. 6 Measured performance of the eletronic filter used to implement direct velocity feedback compared with ideal velocity feedback and a resulting closed-loop transfer function (force excitation at $x/l = 0.2$, deflection sensor at $x/l = 1.0$). Compare with Fig. 2f.

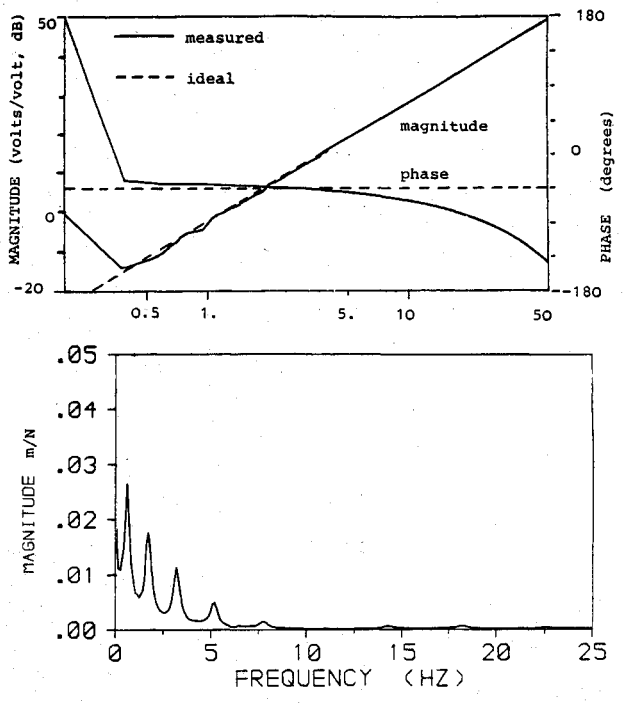

Fig. 7 Measured performance of the electronic filter used to implement the compensator of Eq. (17a), compared to the ideal, and a resulting closed-loop transfer function (force excitation at $x/l=0.2$, deflection sensor at $x/l=1.0$). Compare with Fig. 2c.

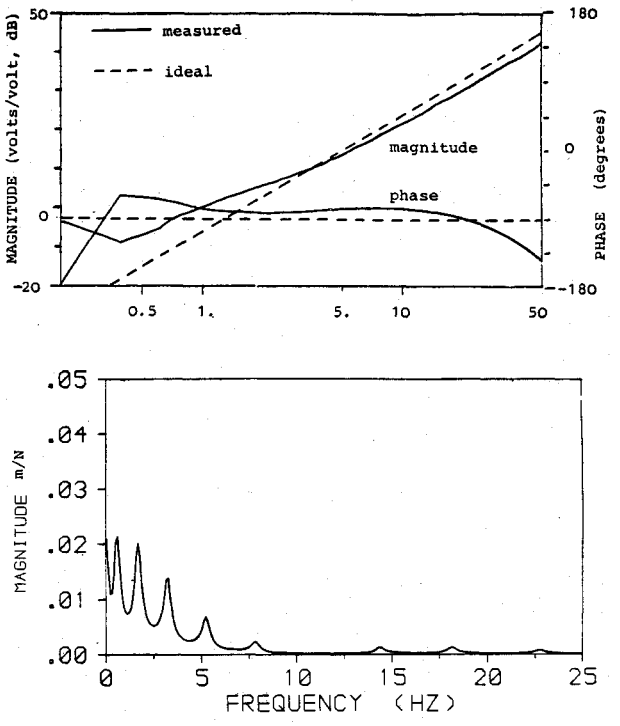

Fig. 8 Measured performance of the electronic filter used to implement the compensator of Eq. (17b), compared to the ideal, and a resulting closed-loop transfer function (force excitation at $x/l=0.2$, deflection sensor at $x/l=1.0$). Compare with Fig. 2d.

loop transfer function may be compred directly with that of Fig. 2f.

The wave-absorbing compensator of Eq. (17a) was implemented without a phase-shifting filter, and with the addition of two 4-pole Butteworth low-pass filters with 200 Hz bandwidth to control noise. The measured compensator transfer function is compared to the ideal in Fig. 7. The $\omega^{3/2}$ (30 dB per decade) gain of the ideal compensator is well approximated, but the phase is poor, due to the low-pass filters used. A lead network could have been used to improve the phase at the expense of the gain. This was not done because the phase deviation is in a direction known to be good for energy dissipation, towards velocity feedback. Figure 7 shows a corresponding closed-loop transfer function. The negative stiffness of this compensator, which originates in the characteristic impedance of the Bernoulli-Euler beam, has seriously degraded the damping at low frequencies. Comparison of this transfer function with the corresponding simulated transfer function of Fig. 2c shows good agreement.

The wave-absorbing compensator of Eq. (17b) was also implemented with the use of two 4-pole Butterworth low-pass filters with bandwidth 200 Hz. The parameters of the phase-shifting circuit were: $K_p=2.34$, $T_a=0$, $T_1=0$, $T_2=0.0419$ s, and $T_3=0.150$ s. A lag network has been used to lag the response at frequencies below 20 Hz. This lag network also reduces the high-frequency gain. As partial compensation, the amplifier gain has been increased. The resulting compromise has too little gain at high frequencies and too much gain at low frequencies. The phase, which should be constant, deviates by as much as 25 deg from the ideal value in the range from 0.5 to 40 Hz. A closed-loop structural transfer function with this compensator active is given in Fig. 8. The closed loop response is very similar to that with velocity feedback (Fig. 5).

The compensator of Eq. (17c) provides by far the best simulated closed-loop response (see Fig. 2e). This compensator was not successfully implemented in the lab. An attempted realization, using the same electronic filter described in the previous paragraph, but with a phase-shifting circuit defined by: $K_p=45.2$, $T_a=0.00398$, $T_1=0.0265$, $T_2=0.00796$ and $T_3=3.18$ s, appeared to be the best approx-

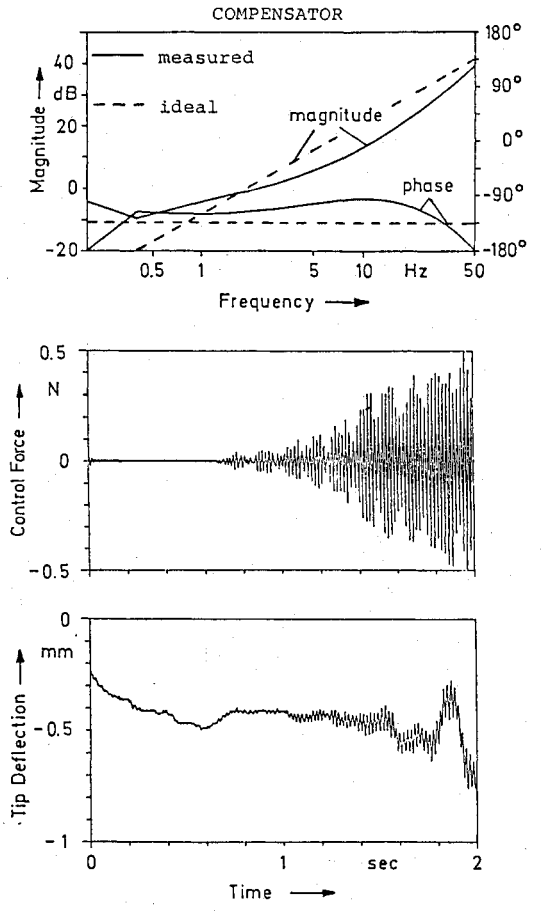

Fig. 9 Measured performance of the electronic filter used to implement the compensator of Eq. (17c), compared to the ideal, and a resulting closed-loop unstable time trace (sensor and actuator at $x/l=1.0$, increasing oscillations from equilibrium position).

imation of the ideal. The compensator transfer function is compared to the ideal in Fig. 9. This compensator destabilized the 15th mode at 53 Hz. The low-frequency behaviour also appeared to be only marginally stable. A typical time trace of the unstable closed-loop system, produced with the compensator of Fig. 9, is also shown.

It is easy to see why this last compensator destabilizes high-frequency modes. A lag-lead network is basically a low-quality band-reject filter, with minimum gain at the frequency of zero phase shift. The use of a lag-lead network to improve the phase reduces the gain strongly at those frequencies where the phase is being affected. To compensate, it is necessary to use very large amplifier gains. Thus, the compensator gain will be much too large at high and low frequencies. The observed instabilities at high frequency and the marginal stability at low frequencies are the consequence.

VI. Conclusions and Discussion

This work has made a strong connection between two very different approaches to the design of low-authority controllers for structural damping augmentation. For the example structure treated, the two procedures lead to control designs which are amazingly similar. The wave-absorbing controllers could be viewed as velocity feedback schemes with frequency dependent gains. This anticipates the effect discovered during the optimization procedure reported.[9] To damp high-frequency modes, the velocity feedback gain must be high, while to damp low-frequency modes, it must be low.

The difficulty encountered in the attempted lab realization of these compensators is also educational. Compensator transfer functions which are derived by some theory may yield a beautiful theoretical response, but this may not be practically achievable. It is not impossible that better lab realizathe wave-absorbing compensator designs can be found, thus enabling more of the performance of the theoretical designs to be achieved. The results of this work are simply that the implementation of such wave-absorbing compensators will require greater sophistication and effort than applied in this study.

Further work is planned in the development of wave-shunting compensators for structural junctions. Disturbance propagation in, and compensator design for, periodic truss-work beams is under study. These compensators are strongly influenced by the mechanical filtering behavior of such beams. Simplifications of "perfect" wave-absorbing and wave-shunting compensators will always be possible. Such simplifications will be based upon detailed analysis and understanding of local dynamics and of the disturbance-propagation behaviour of the components involved.

Acknowledgments

This work was performed while the first author was on study visit to the DFVLR Oberpfaffenhofen. The study visit was made possible by a fellowship of the Alexander von Humboldt-Stiftung, by the hospitality of the DFVLR and the section head, Dr. Konrad Reinel, and by the administrative aid of Prof. Argyris of Stuttgart University. The work would not have been practicable in the short time it was performed without the existence of the experimental structure, sensors, and actuators. A great deal of development effort had been invested in the actuators and structure by Dr. Reinel's section in the previous three years, notably by H. Holzach and Th. Lange. The previous work of G. Schulz and G. Heimbold in the design of optimized direct-velocity feedback provided a guide for the execution of these experiments, and a performance baseline for comparison of results. The electronic filter was built and tested by C. Mietner at the DFVLR.

References

[1]Gupta, N.K., Lyons, M.G., Aubrun, J.-N., and Margulies, G., "Modelling, Control and System Identification Methods for Flexible Structures," in AGARDograph-AG-260, 1981.

[2]Aubrun, J-N., "Theory of the Control of Structures by Low-Authority Controllers," *Journal of Guidance, Control, and Dynamics,* Vol. 3, Sept.-Oct. 1980, pp. 444-451

[3]Balas, M.J., "Direct Velocity Feedback Control of Large Space Structures," *Journal of Guidance, Control, and Dynamics,* Vol. 2, pp. 252-253, May-June 1979.

[4]Schultz, G., Heimbold, G., "Dislocated Actuator/Sensor Positioning and Feedback Design for Flexible Structures," *Journal of Guidance, Control, and Dynamics,* Vol. 6, Sept.-Oct. 1983, pp. 361-367.

[5]Aubrun, J-N., Magulies, G., "Low-Authority Control Synthesis for Large Space Structures," NASA Contractor Report, Contract NAS1-14887-Task 11, May 1982.

[6]von Flotow, A.H., "Travelling Wave Control for Large Spacecraft Structures," to appear in *Journal of Guidance, Control, and Dynamics.*

[7]von Flotow, A.H., "Disturbance Propagation in Structural Networks; Control of Large Space Structures," PhD. Dissertation, Stanford University, Stanford, CA, June 1984.

[8]Aubrun, J-N, Gregory, C.Z., Lyons, M.G., Kosut, R.L., and Woods Jr., A.A., "Vibration Control of Space Structures VCOSS A: High and Low-Authority Hardware Implementations," AFWAL-TR-83-3074, July 1983.

[9]Schäfer, B., and Holzach, H., "Experimental Research on Flexible Beam Modal Control," *Journal of Guidance, Control, and Dynamics,* Vol. 8, Sept.-Oct. 1985, pp. 597-604.

[10]Collatz, L., "Eigenwertaufgaben mit technischen Anwendungen," Akademische Verlagsgesellschaft, Leipzig, 1949.

[11]Steele, C.R., "Application of the WKB Method in Solid Mechanics," *Mechanics Today,* Vol. 3, 1976, pp. 243-295.

[12]Ghose, R.H., *Microwave Circuit Theory and Analysis,* McGraw-Hill, 1963.

[13]Vaughan, D.R., "'Application of Distributed Parameter Concepts to Dynamic Analysis and Control of Bending Vibrations," *Journal of Basic Engineering,* June 1968, pp. 157-166.

[14]Carlson, G.E. and Halijak, C.A., "Simulation of the Fractional Derivative Operator $\sqrt{s}$ and the Fractional Integral Operator $1/\sqrt{s}$", Kansas State University Bulletin, Vol. 45, July 1961, pp. 1-22.

[15]Herrmann, O., "Transversalfilter zur Hilbert-Transformation," *Archiv der Elektrischen Übertragung,* Band 23, Heft 12, DC 1969, 561-587.

[16]Herrmann, O., "Quadraturfilter mit rationalem Übertragungsfaktor," *Archiv der Elektrischen Übertragung,* Band 23, Heft 2, Feb. 1969, pp. 77-84.